敏化处理对 2209 双相不锈钢堆焊层点蚀行为的影响

柳昱[1], 包晔峰[1,2], 宋亓宁[1], 蒋永锋[1]
(1. 河海大学, 常州, 213000; 2. 河海大学, 疏浚技术教育部工程研究中心, 常州, 213000)

摘要: 在 850 ℃ 下, 对 2209 双相不锈钢堆焊试样进行不同时间 (15 min, 30 min, 1 h, 2 h) 的敏化处理. 通过浸泡试验和交流阻抗试验研究了敏化时间对 2209 双相不锈钢堆焊层耐点蚀性能的影响. 结果表明, 对于不同时间敏化处理的试样, 点蚀均起源于铁素体相; 点蚀速率与敏化时间相关, 敏化处理时间小于 30 min 时, 堆焊层的点蚀失重不明显, 当敏化时间大于 30 min 时, 点蚀失重量明显上升. 阻抗谱结果显示容抗弧曲率半径随着敏化时间的增加呈不断减小的趋势, 说明钝化膜的稳定性下降, 耐点蚀性能下降, 与浸泡试验的结果吻合.

关键词: 2209 双相锈钢堆焊层; 敏化处理; 点蚀
中图分类号: TG 455 **文献标识码:** A **doi:** 10. 12073/j. hjxb. 20200331004

0 序言

双相不锈钢是微观组织由铁素体和奥氏体两相组成的重要工程结构用钢, 其两相比例接近于 1∶1, 一般较少相的含量也要达到 30% 以上. 因此, 它兼有铁素体不锈钢良好的耐氯化物应力腐蚀性能和高强度的优势, 以及奥氏体不锈钢优良的韧性和易焊接等优点, 广泛应用于存在氯离子的加工工业、石油化工、造纸、化肥以及海水等环境[1-4].

双相不锈钢的发展趋势是提高 Cr 和 Mo 的含量, 以提高其耐腐蚀性能. 然而, 高的 Cr 和 Mo 含量也降低了双相不锈钢的组织稳定性. 在焊接以及不正当的热处理时, 焊接接头微区的亚稳态热力学平衡被打破, 有通过金属间相 (σ, χ), 碳化物 ($M_{23}C_6$, M_7C_3) 的析出达到新的热力学稳定的趋势, 而金属间相的析出降低了双相不锈钢的耐局部腐蚀性能[5].

2209 双相不锈钢在 600 ~ 950 ℃ 的温度区间内, χ 相、σ 相会在铁素体-奥氏体相界或铁素体相内析出, 引起局部 Cr 贫化, 影响钝化膜的均匀性, 促进点蚀的发生[6]. 而在 2209 双相不锈钢堆焊及焊后冷却的过程中, 并不能避免在此温度区间停留, 造成上述相的析出, 严重影响材料的性能. 因此, 在生产和使用过程中控制有害析出相的形成是一个至关重要的环节. 所以, 研究的目的在于通过研究敏化处理对 2209 双相不锈钢 TIG 堆焊层组织和性能的影响, 为 2209 双相不锈钢的堆焊工艺的制定和优化提供理论指导.

1 试验方法

1.1 试验材料

基底板材为 304 奥氏体不锈钢, 板材厚度为 3 mm, 其化学成分如表 1 所示. 堆焊焊材为 ER2209 焊丝, 焊丝直径为1.2 mm, 其化学成分如表 2 所示.

表 1 基底板材化学成分 (质量分数, %)
Table 1 Chemical composition of base plate

C	Si	Mn	P	S	Cr	Ni	N	Fe
≤ 0.08	≤ 1.0	≤ 2.0	≤ 0.03	≤ 0.03	18.0 ~ 20.0	8.0 ~ 10.5	≤ 0.1	余量

1.2 TIG 堆焊

采用威特力焊机公司生产的 WS−315 IGBT 逆变直流氩弧焊机, 采用 ER2209 焊丝在 304 奥氏体

收稿日期: 2020 − 03 − 31
基金项目: 国家自然科学基金资助项目 (51879089); 中央高校基本科研业务费专项资金资助 (B200204036).

不锈钢上堆焊出 6 ~ 8 mm 厚的堆焊层. 保护气体为氩气, 其纯度 ⩾ 99.99%. 在焊接过程中, 为防止堆焊层在高温停留时间过长, 使用测温枪进行监测, 确保上道焊缝空冷至 100 ℃ 以内后再进行下道堆焊, 严格控制层间温度在 100 ℃ 以内. TIG 焊堆焊工艺参数如表 3 所示.

表 2 ER2209 焊丝化学成分 (质量分数, %)

Table 2 Chemical composition of ER2209 welding wire

C	Si	Mn	P	S	Cr	Mo	Ni	N	Fe
0.02	0.55	1.55	0.012	0.008	22.5	3.3	8.55	0.2	余量

表 3 TIG 焊堆焊的焊接工艺参数

Table 3 Welding parameters of TIG

堆焊层数	焊接电流 I/A	电弧电压 U/V	焊接速度 v/(m·min^{-1})	保护气流量 q/(L·min^{-1})	钨极直径 d/mm
第一层	90	13	0.09	8	1.6
第二层	110	15	0.18	10	1.6
第三层	110	15	0.18	10	1.6

1.3 固溶处理

将试样在 TCXC-1700 马弗炉中加热 120 min 至 1 100 ℃, 保温 60 min 后, 以水冷的方式快速冷却.

固溶处理的目的是将堆焊层中的析出相固溶到基体当中并调整铁素体与奥氏体的相比例, 使两相比例接近 1∶1, 从而提高 2209 双相不锈钢 TIG 堆焊层的强度、韧性以及耐蚀性能[3].

1.4 敏化处理

将试样在 TCXC-1700 马弗炉中加热 90 min 至 850 ℃, 分别保温 15 min, 30 min, 1 h 和 2 h, 随后采用水冷的方式快速冷却以研究不同时长的敏化处理对 2209 双相不锈钢 TIG 堆焊层的组织和性能的影响.

1.5 浸泡试验

将敏化处理过后的 30 mm × 20 mm × 5 mm 的试样浸泡在 1 L 10% $FeCl_3$ + 2% HCl 溶液中, 每隔 24 h 取出吹干称重并对试样表面腐蚀形貌拍照记录, 总浸泡时长 72 h.

1.6 交流阻抗试验

电化学测试设备为 AUTOLAB (PGSTAT302N 瑞士万通), 采用标准三电极体系, 2209 双相不锈钢堆焊层作为工作电极, 饱和甘汞电极 (SCE) 作为参比电极, 碳电极作为辅助电极. 电化学阻抗谱 (EIS) 在开路电位下测试, 频率范围为 100 ~ 0.01 Hz, 交流激励信号幅值为 10 mV.

2 试验结果和分析

2.1 固溶处理试验的组织形貌

采用 40 mL H_2O + 8 g $K_3[Fe(CN)_6]$ + 8 g KOH 对试样进行蚀刻, 焊态和固溶处理后堆焊层的显微组织形貌如下图 1 所示. 浅色部分为奥氏体组织, 深色部分为铁素体组织. 焊态下的显微组织如图 1a 所示, 在铁素体相内以及铁素体−奥氏体相界处, 存在有少量的黑色析出相. 这是因为在堆焊的过程中, 后续焊道对先前形成的焊道有再加热的效果, 堆焊层在高温区的停留时间过长, 焊后冷却速度不够快而导致析出相的形成[4]. 由于文中采用热输入比较小的 TIG 焊来进行堆焊, 并且对层间温度进行了控制, 因而析出相的数量很少. 固溶处理后的显微组织如图 1b 所示, 在固溶处理后, 铁素体相的比例增大, 堆焊层晶粒尺寸变得更加细小, 铁素体相和奥氏体相的晶界变得明显且两相组织的分布更加均匀. 另外, 在焊态的堆焊层组织中, 只有少部分的铁素体分布在奥氏体相内, 大部分的铁素体分布在奥氏体的晶界处; 而在焊后经过固溶处理的堆焊层组织中, 铁素体则近乎全部位于奥氏体的晶界处, 几乎没有在奥氏体相内分布.

2.2 敏化处理后组织形貌和分析

经不同时间 (15 min, 30 min, 1 h, 2 h) 敏化处

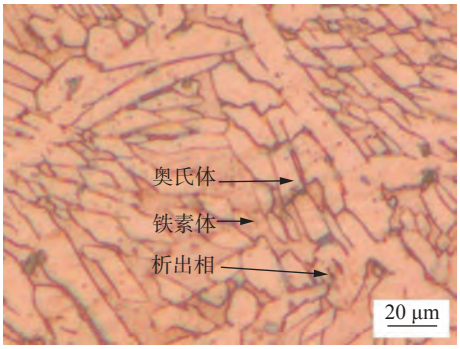

(a) 焊后组织

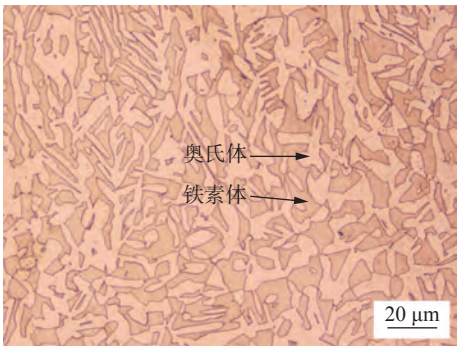

(b) 固溶处理后组织

图 1　2209 双相不锈钢堆焊层显微组织

Fig. 1　Microstructure of 2209 duplex stainless steel surfacing layer. (a) weld microstructure; (b) solid solution microstructure

理的 2209 双相不锈钢堆焊试样的显微组织如图 2 所示. 从图 2a 可以看出，敏化 15 min 后，在铁素体晶界以及铁素体–奥氏体相界面处出现了大量黑色的析出相，且铁素体的含量较固溶处理后有所下降. 当敏化时间为 30 min (图 2b) 时，可以看到析出相明显增多并形成断续的条状组织，铁素体的含量进一步减少. 当敏化时间为 1 h (图 2c) 时，条状析出相的含量进一步增加，尺寸也显著增大，形成较为连续的片状. 当敏化时间为 2 h (图 2d) 时，析出相形成连续的片状，铁素体相含量极少.

通过相比例分析发现，随着敏化处理时间的增加，奥氏体相和黑色析出相的比例增大，而铁素体相的比例则呈现显著减少的趋势. 这是因为，在 850 ℃ 下敏化处理时，随着敏化时间的增加，铁素体通过共析反应的方式转变为 σ 相和二次奥氏体 γ_2，即 $\alpha \rightarrow \sigma + \gamma_2$，由此可知黑色析出相为 σ 相，而二次奥氏体 γ_2 会附着在初始奥氏体 γ_1 上. 随着敏化处理时间的延长，整个组织将有一次奥氏体 γ_1、二次奥氏体 γ_2 和 σ 相组成.

2.3　浸泡试验结果和分析

堆焊层的耐点蚀性能可以通过腐蚀速率来评价，即单位面积、单位时间内的失重. 试验结果见表 4. 腐蚀速率(g/(m^2·h))可表示为

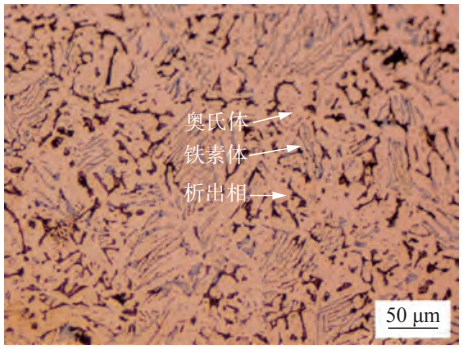

(a) 敏化 15 min

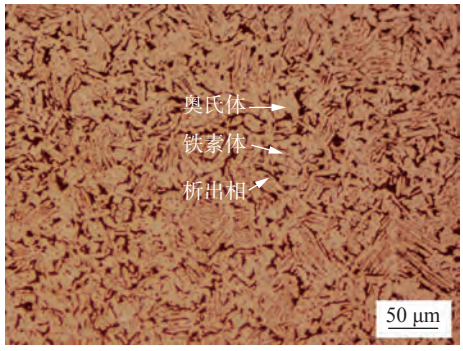

(b) 敏化 30 min

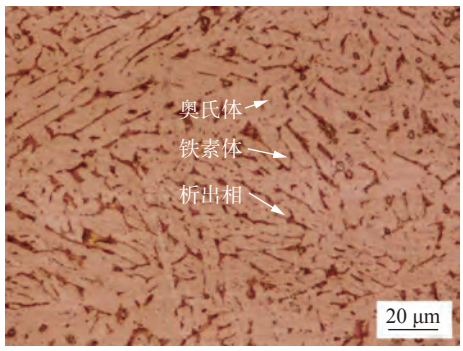

(c) 敏化 1 h

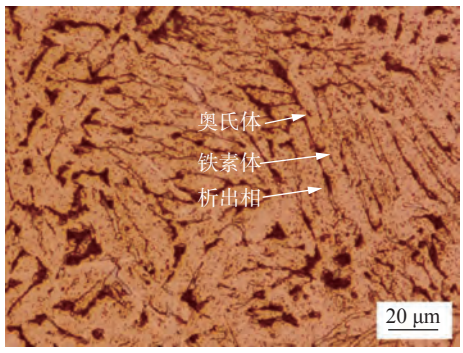

(d) 敏化 2 h

图 2　2209 双相不锈钢堆焊层经 850 ℃ 敏化处理不同时长后的显微组织

Fig. 2　Microstructure of 2209 duplex stainless steel surfacing layer sensitized at 850 ℃ for different times. (a) sensitization 15 min; (b) sensitization 30 min; (c) sensitization 1 h; (d) sensitization 2 h

表 4 浸泡试验结果 (10% $FeCl_3$ + 2% HCl，20 ℃，72 h)

Table 4 Immersion test results (10% $FeCl_3$ + 2% HCl, 20 ℃, 72 h)

试样	试样尺寸 V/mm^3	试验前重量 W_1/g	浸泡24 h后重量 W_2/g	浸泡48 h后重量 W_2/g	浸泡72 h后重量 W_2/g	腐蚀速率 v/(g·m^{-2}·h^{-1})
敏化 15 min	29.45 × 19.48 × 5.41	23.85	23.84	23.83	23.80	0.414
敏化 30 min	29.28 × 19.52 × 5.38	23.72	23.69	23.65	23.59	1.082
敏化 1 h	29.58 × 19.50 × 5.36	24.06	23.95	23.64	23.25	6.697
敏化 2 h	29.57 × 19.47 × 5.36	23.84	23.59	23.24	22.56	10.600

$$v = \frac{W_1 - W_2}{S \cdot t} \tag{1}$$

式中：v 为腐蚀速率；W_1 为试验前的试样重量 (g)；W_2 为试验后的试样重量 (g)；S 为试样表面积 (m^2)；t 为浸泡时间 (h).

2209 双相不锈钢堆焊层敏化处理后试样在 10% $FeCl_3$ + 2% HCl 的腐蚀介质当中浸泡 72 h 的失重情况如图 3 所示，宏观形貌如图 4 所示. 敏化处理 15 min 和 30 min 的堆焊层试样的腐蚀速率较慢，失重量随浸泡时间的延长呈现略微增加的趋势. 敏化 1 h 和 2 h 的堆焊层试样的失重量随浸泡时间的延长而不断增加且增幅明显. 说明随着堆焊

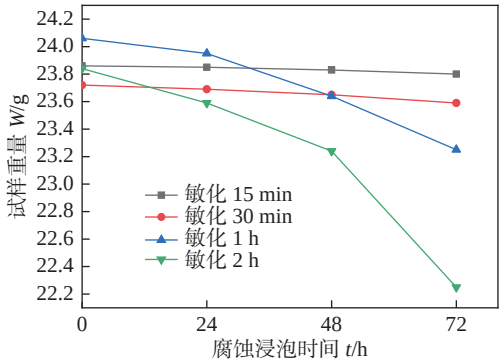

图 3 不同敏化处理样品在 10% $FeCl_3$ + 2% HCl 中浸泡失重结果

Fig. 3 Results of different sensitized samples immersed in 10% $FeCl_3$ + 2% HCl

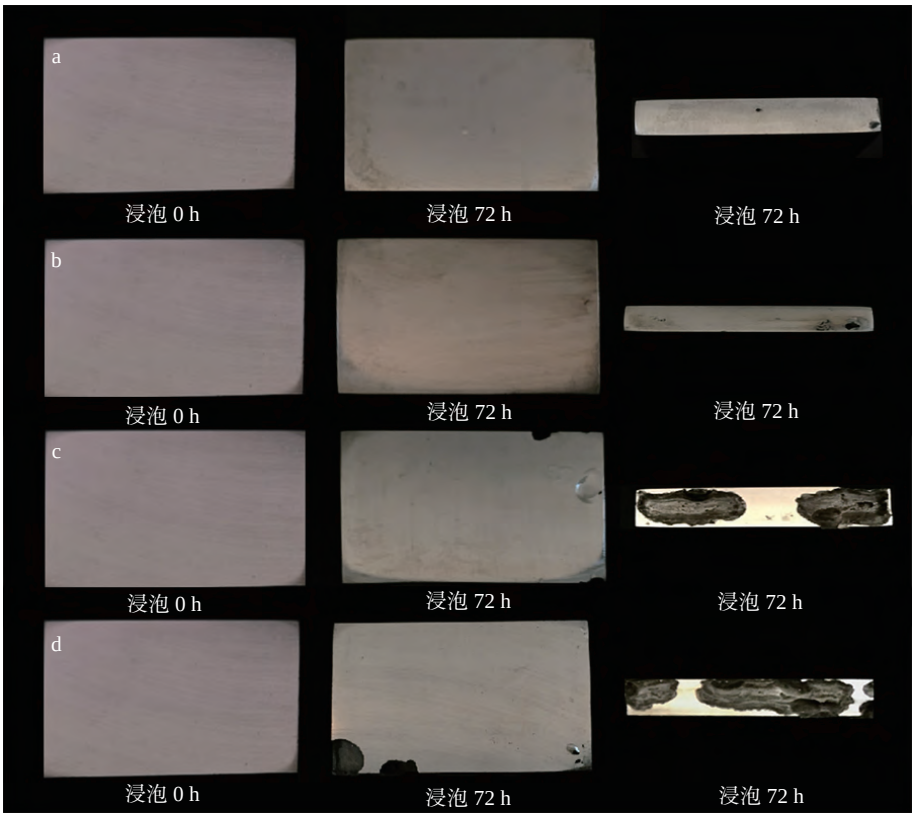

图 4 试样在 10% $FeCl_3$ + 2% HCl 中浸泡 72 h 的宏观形貌 (a, b, c, d 分别为敏化 15 min, 30 min,1 h, 2 h 的试样)

Fig. 4 Macromorphology of different sensitized samples soaked in 10% $FeCl_3$ + 2% HCl, for 72 h

层敏化处理时间的增加，堆焊层试样的点蚀性能不断下降，并且当敏化处理的时长超过 30 min 以后，耐点蚀性能严重下降.

点蚀性能下降是因为随着敏化处理时间的增加，析出相 σ 相的含量不断增加，由于 σ 相中 Cr 含量的富集，致使其周围区域的 Cr 含量减少，形成贫 Cr 区，导致钝化膜稳定性变差，且不均匀，易形成微观化学电池，促进点蚀的发生.

2.4　交流阻抗试验结果

双相不锈钢具有优越的耐腐蚀性，这与它表面形成的钝化膜密切相关. 一般认为，双相不锈钢表面形成的钝化膜具有两层结构[7]. 致密的内层称为阻挡层，主要由铬，镍的氧化物构成，多孔外层主要由氧化铁和氢氧化物组成. 但是，双相不锈钢在敏化处理的过程中会析出 σ 相，从而导致析出相周围形成贫 Cr 区，使得钝化膜减薄，易破坏，发生局部腐蚀[8].

图 5 是在室温下，经过不同时长敏化处理的 2209 双相不锈钢堆焊层在 3.5% NaCl 溶液中的交流阻抗谱. 从图中可以直观的看出敏化处理 15 min 的堆焊层试样其容抗弧半径最大，表明其阻抗最大，耐蚀性最好，而敏化处理达 2 h 的堆焊层试样其容抗弧半径最小，意味着它的耐蚀性最差. 且随着敏化时间的增长，堆焊层的容抗弧半径逐渐减小，堆焊层耐蚀性逐渐变差. 但敏化处理 30 min 的 2209 双相不锈钢堆焊层试样其容抗弧半径较敏化处理 15 min 的试样减小不明显，说明敏化处理时长在 30 min 内，对试样耐点蚀性能的影响不大，这也与浸泡试验的结果相对应.

采用软件 ZView 对交流阻抗谱进行拟合，拟合电路如图 6 所示，其中 R_s 指溶液的电阻；R_{ct} 指为电荷转移电阻；CPE 为双电层电容；n 为弥散效应指数，n 越接近 1，表明钝化膜的完整性越强[9]. 对不同敏化处理时间的堆焊层试样的电化学阻抗谱数据进行整合并通过等效电路拟合，得到了 4 种敏化

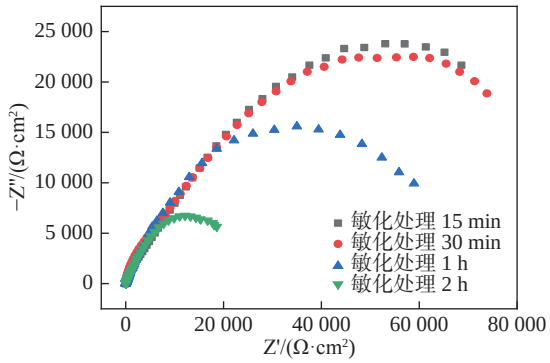

图 5　经过不同时长敏化处理的 2209 双相不锈钢堆焊层在 3.5% NaCl 溶液中的阻抗谱

Fig. 5　Electrochemical impedance spectroscopy for 2209 duplex stainless steel in 3.5% NaCl solution after sensitization for different times

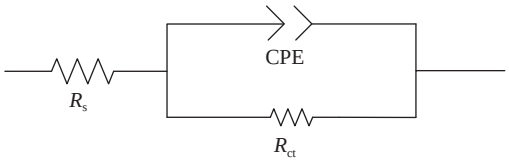

图 6　交流阻抗谱对应的等效电路

Fig. 6　Equivalent circuit of electrochemical impedance spectroscopy

处理时间的 2209 双相不锈钢堆焊层数据如表 5 所示. 由表 5 的拟合数据可见，随着敏化处理时间的延长，R_{ct} 的数值不断减小，意味着电荷穿越双电层的阻力越小，堆焊层试样的表面活性增大. 其中敏化 15 min 试样的 R_{ct} 是敏化 30 min 试样的 2.29 倍，是敏化 1 h 试样的 5.05 倍，是敏化 2 h 试样的 8.08 倍，意味着堆焊试样表面活性在敏化时间为 30 min 之内时缓慢增大，30 min 后快速增大. n 的值同样随敏化处理时间的延长而变小，表明随着敏化处理时间的延长，钝化膜的膜电阻减小，稳定性变差，从而导致耐蚀性能减弱.

在 3.5% NaCl 溶液中，四组经过不同时长敏化处理的堆焊层试样的耐腐蚀能力由强到弱的排序情况为：敏化 15 min > 敏化 30 min > 敏化 1 h > 敏化 2 h. 所以，在 3.5% 的 NaCl 溶液中，2209 双相

表 5　2209 双相不锈钢堆焊层 EIS 等效电路拟合数据

Table 5　EIS equivalent circuit fitting data of 2209 duplex stainless steel surfacing layer

试样	溶液电阻 R_s/(Ω·cm²)	双电层电容 CPE-T/(10^{-5}F·cm^{-2})	弥散效应指数 n	电荷转移电阻 R_{ct}/(Ω·cm²)
敏化 15 min	8.168	2.33	0.837	2721.0
敏化 30 min	11.260	1.92	0.811	1190.0
敏化 1 h	9.516	2.49	0.728	539.3
敏化 2 h	6.385	2.51	0.571	336.6

不锈钢堆焊层的耐点蚀性能随敏化处理时间的增加而降低，且敏化处理时间在 30 min 内时，试样的耐点蚀性能减弱缓慢，当敏化处理时间大于 30 min 时，试样的耐点蚀性能快速减弱.

3 结论

(1) 2209 双相不锈钢堆焊过程中应严格把控焊缝的冷却速度，确保层间温度低于 100 ℃，减少析出相析出，以获得性能优良的双相组织.

(2) 2209 双相不锈钢堆焊层试样在 850 ℃ 下进行敏化处理，敏化 15 min 时，已经有明显的 σ 相在铁素体晶界和铁素体−奥氏体相界面处形成，σ 相是铁素体相发生共析反应生成的，即 $\alpha \rightarrow \sigma + \gamma_2$. 且 σ 相随敏化处理时间的增加而逐渐布满铁素体相，直至铁素体相分解完全.

(3) 浸泡试验表明，敏化处理时间在 30 min 内时，2209 双向不锈钢堆焊层的点蚀失重不明显；当敏化时间超过 30 min 后，点蚀速率明显上升. 随着敏化处理时间的延长，2209 双相不锈钢堆焊层耐点蚀性能降低.

(4) 交流阻抗试验表明，随着敏化处理时间的延长，2209 双相不锈钢堆焊层试样的容抗弧半径不断减小，说明钝化膜的稳定性不断下降，耐点蚀性能逐渐降低，但敏化处理时间在 30 min 内时，其容抗弧半径减小缓慢.

参考文献

[1] 高娃, 罗建民, 杨建君. 双相不锈钢的研究进展及其应用 [J]. 兵器材料科学与工程, 2005, 28(3): 61 − 64.
Gao Wa, Luo Jianmin, Yang Jianjun. Research progress and application of double phase stainless steel[J]. Ordnance Material Science and Engineering, 2005, 28(3): 61 − 64.

[2] 吴玖, 刘尔华. 国内外双相不锈钢材料和应用的发展 [J]. 不锈钢, 2010(1): 1 − 8.
Wu Jiu, Liu Erhua. Development of duplex stainless steel materials and applications at home and abroad[J]. China Stainless, 2010(1): 1 − 8.

[3] 伍曦耘. 2205 双相不锈钢固溶处理工艺研究 [J]. 大型铸锻件, 2009(4): 16 − 18, 21.
Wu Xiyun. The technical study of 2205 duplex stainless steel solid solution treatment[J]. Heavy Casting and Forging, 2009(4): 16 − 18, 21.

[4] 张建勋, 李为卫, 李庆琰. 2205 双相不锈钢的焊接性研究综述 [J]. 焊管, 2005(5): 6 − 10, 89.
Zhang Jianxun, Li Weiwei, Li Qingyan. State of the art weldability of the 2205 duplex stainless steel[J]. Welded Pipe and Tube, 2005(5): 6 − 10, 89.

[5] 晁代义, 徐仁根, 孙有政, 等. 850 ℃ 时效处理对 2205 双相不锈钢组织与力学性能的影响 [J]. 材料导报, 2019, 33(s1): 369 − 372.
Chao Daiyi, Xu Rengen, Sun Youzheng, *et al*. Effect of aging treatment at 850 ℃ on microstructures and mechanical properties in duplex stainless steel 2205[J]. Materials Reports, 2019, 33(s1): 369 − 372.

[6] 孙立. σ 相析出对双相不锈钢点蚀性能影响及其机理 [D]. 马鞍山: 安徽工业大学, 2017.
Sun Li. Effect of σ phase precipitation on pitting properties of duplex stainless steel and its mechanism[D]. Ma Anshang: Anhui University of Technology, 2017.

[7] Fernández-Domene R M, Blasco-Tamarit E, García-García D M, *et al*. Effect of alloying elements on the electronic properties of thin passive films formed on carbon steel, ferritic and austenitic stainless steels in a highly concentrated LiBr solution[J]. Thin Solid Films, 2014, 558: 252 − 258.

[8] Leiva-García R, Fernandes J C S, Muñoz-Portero M J, *et al*. Study of the sensitisation process of a duplex stainless steel (UNS 1.4462) by means of confocal microscopy and localised electrochemical techniques[J]. Corrosion Science, 2015, 94: 327 − 341.

[9] Dong Chaofang, Luo Hong, Xiao Kui, *et al*. Effect of temperature and Cl^- concentration on pitting of 2205 duplex stainless steel[J]. Wuhan University of Technology, 2011, 26(4): 641 − 647.

第一作者简介：柳昱，1995 年出生，硕士研究生；主要从事双相不锈钢耐腐蚀耐空蚀方向的研究. Email: 980560463@qq.com.

通信作者简介：包晔峰，教授. Email: baoyf@hhuc.edu.cn.

（编辑： 周珍珍）

solve the problems were put forward through applying a synchronous magnetic field. The effect of the synchronous magnetic field with different types on arcing phase was investigated. The short-circuit transfer processes were captured through high-speed camera system with laser backlight to observe the droplet transfer process, calculate droplet size and transfer frequency, etc. The experimental results showed that the droplet transfer frequency was increased, the short-circuit metal transfer process was more stable, the shape of droplet was changed evidently from a round or ellipsoid with sharp tip to flat end, and the dimension of droplet was reduced.

Key words: short-circuit transfer; synchronous magnetic field; CO_2 arc welding; droplet transfer frequency; the morphology of droplet

Effect of solid lubricant on contact tip wear performance of non-copper coated solid wire CAO Xiaotao[1], LI Zhuoxin[1], Wolfgang Tillmann[2], Meng bo[3], Qiao Jichun[3]
(1. Beijing University of Technology, Beijing, 100124, China; 2. Dortmund University of Technology, Dortmund, 44227, China; 3. JULI Welding Material Co., Ltd., Shandong, 253000, China). pp 22-27

Abstract: The effects of solid lubricants on contact tip wear performance of non-copper coated solid wire were investigated by scanning electron microscopy (SEM) and stereoscopic microscope. It was found that the wear form of contact tip varied with composition of solid lubricant, therefore, the mass and aperture wear loss rate of contact tip were changed. When surface coatings of non-copper coated solid wire were mainly composed of graphite + nano Fe_2O_3, the mass and aperture wear loss rate of contact tip were 0.27%, 16.2%, respectively. Coated with graphite + nano Fe_3O_4, contact tip wear perfermance of non-copper coated solid wire were better, the mass and aperture wear loss rate wear of contact tip were 0.31%, 22.3%, respectively. Slight abrasive wear was wear form of contact tip. Contact tip temperature had an important role on the lubricity of solid lubricants, the solid lubricants mainly composed of graphite + nano Fe_2O_3 or graphite + nano Fe_3O_4 can achieve continuous lubrication from room temperature to higher temperature range.

Key words: non-copper coated solid wire; contact tip wear; solid lubricant; contact tip temperature

Bead geometry measurement for wire and arc additive manufacturing using active-passive composite vision sensing based on regional filter HAN Qinglin[1], LI Dayong[2], LI Xinlei[1], HAN Changle[1], ZHANG Guangjun[1]
(1. State Key Laboratory of Advanced Welding and Joining, Harbin Institute of Technology, Harbin Institute of Technology, Harbin 150001, China; 2. Bohai Shipyard Group Co., Ltd, huludao, 125003, China). pp 28-32

Abstract: An active-passive composite vision sensing system was designed to overcome the delay of active vision sensing and limited information on passive vision sensing. To capture the high brightness molten pool and low brightness structured light clearly in one image, a regional dimming method was proposed to make their brightness decline to the same level. Lightpath analysis showed that the regional dimming filter must be placed in front of the focal point before the lens, or between the CCD sensor and the focal point behind the lens. The molten pool and structured light have been clearly presented in one image using this system. An image processing algorithm for online measurement of bead geometries is proposed. The experimental results showed that the measurement error of bead height is less than 0.1 mm, and that of bead width is less than 0.2 mm.

Key words: wire and arc additive manufacturing; regional dimming; active-passive composite vision sensing; bead geometries

Influence of sensitization on pitting corrosion in surfacing layer of 2209 duplex stainless steel LIU Yu[1], BAO Yefeng[1,2], SONG Qining[1], JIANG Yongfeng[1] (1. Hohai university, Changzhou, 213000, China; 2. Engineering Research Center of Dredging Technology of Ministry of Education, Hohai University, Changzhou, 213000, China). pp 33-38

Abstract: The sensitization of 2209 duplex stainless steel surfacing layer was processed in different time (15 min, 30 min, 1 h, 2 h) under 850 ℃, and the influence of sensitization time on the pitting resistance of 2209 duplex stainless

steel surfacing layer was studied by immersion experiment and EIS. These results showed that pitting corrosion originated from the ferrite phase in different time sensitized sample. Moreover, the pitting corrosion rate was correlated with the sensitization time, if sensitizing processing time was less than 30 min, pitting corrosion weightlessness of surfacing layer was not obvious, while it longer than 30 min, pitting corrosion weightlessness would increase obviously. The EIS supported, with the increasing of sensitization time, capacitive reactance curvature radius would decrease continuously. Which indicated that both the stability of the passive film and pitting resistance were decreased, being similar with the result of immersion experiment.

Key words: surfacing layer of 2209 duplex stainless steel; sensitization; pitting corrosion

Effect of ultrasonic impact time on VPPA-MIG welded joint of 7A52 aluminum alloy CHEN Furong, LIU Chenghao, LI Nan (School of Materials Science and Engineering, Inner Mongolia University of Technology, Hohhot, 010051, China). pp 39-43

Abstract: In order to study the effect of ultrasonic impact time on microstructure and properties of VPPA-MIG composite welded joint of 7A52 aluminum alloy, ultrasonic impact treatment of 2.5, 5, 10, 15, 30, and 75 min was carried out on the welded joint per unit area. By observing the surface morphology of the joint and testing the mechanical properties of the joint, the effect of ultrasonic impact treatment time on the joint was analyzed. The results show that the surface of 7A52 aluminum alloy welded joint is obviously strengthened after ultrasonic impact treatment. The grain size of weld surface reaches 26.28 nm when ultrasonic impact time is 15 min; the hardness of weld surface is 138.8 HV when ultrasonic impact time is 75 min, which is 36.3% higher than that of original weld; the maximum residual compressive stress is 243.3 MPa after ultrasonic impact treatment for 30 min.

Key words: ultrasonic impact treatment; aluminum alloy; VPPA-MIG; microstructure; mechanical properties

Effect of Pt modification on oxidation properties and microstructure of NiAl coatings HAN Zhiyong, LU Bowen, WANG Shicheng (Tianjin Key Laboratory for Civil Aircraft Airworthiness and Maintenance, Civil Aviation University of China, Tianjin, 300300, China). pp 44-48

Abstract: NiAl coatings was fabricated on Hastelloy X substrate by atmospheric plasma spraying technique, and Pt was electroplated on NiAl coatings and vacuum diffusion was performed to prepare high performance Ni-Al-Pt coatings. High temperature oxidation tests were carried out on NiAl coatings and Pt modified coatings to observe and analyze the oxidation behavior, phase composition and microstructure of the two coatings. The oxidation kinetic curve results show that, compared with the NiAl coatings, the oxidation kinetics curve of the modified coating is closer to the parabola, and the weight gain in the late oxidation period is slower. XRD results show that the Pt modified coating can quickly form a continuous and dense Al_2O_3 film on the surface at the initial stage of oxidation. When it is oxidized to 90 h, the coating surface is still mainly α-Al_2O_3. The SEM results showed that after Pt modified coating oxidation for 30 min, a mixed structure of θ-Al_2O_3 and α-Al_2O_3 appeared on the surface of the coating. After the coating was oxidized for 35 h, the θ-Al_2O_3 basically transformed into continuous and dense α-Al_2O_3. When the coating is oxidized for 90 h, the coating surface is mainly composed of sheet-like α-Al_2O_3 and agglomerated NiO, the coating still has higher oxidation resistance.

Key words: Ni-Al-Pt coatings; oxidation behavior; phase composition; microstructure; thermally grown oxide

Experimental research on the blind hole-drilling method for measuring residual stress of steel plate HUANG Gang, ZHANG Qingdong, WANG Chunhai, ZHANG Boyang, KONG Ning (School of Mechanical Engineering, University of Science and Technology Beijing, Beijing, 100083, China). pp 49-59,80

Abstract: The blind hole method is the most widely non-destructive measurement method to measure the residual stress. In order to use the blind hole method more reasonable